NJC

Accepted Manuscript

This is an *Accepted Manuscript*, which has been through the Royal Society of Chemistry peer review process and has been accepted for publication.

Accepted Manuscripts are published online shortly after acceptance, before technical editing, formatting and proof reading. Using this free service, authors can make their results available to the community, in citable form, before we publish the edited article. We will replace this *Accepted Manuscript* with the edited and formatted *Advance Article* as soon as it is available.

You can find more information about *Accepted Manuscripts* in the Information for Authors.

Please note that technical editing may introduce minor changes to the text and/or graphics, which may alter content. The journal's standard Terms & Conditions and the Ethical guidelines still apply. In no event shall the Royal Society of Chemistry be held responsible for any errors or omissions in this *Accepted Manuscript* or any consequences arising from the use of any information it contains.

ROYAL SOCIETY OF CHEMISTRY

www.rsc.org/njc

Synthesis and characterization of core/shell/shell magnetic ($CoFe_2O_4/SiO_2/TiO_2$) nanocomposite and TiO_2 nanoparticle for photocatalytic activity under UV and visible irradiation.

Hesham Hamad[1,2*], Mona Abd El-Latif [1], Abd El-Hady Kashyout[3], Wagih Sadik[4], Mohamed Feteha[4]

[1] Fabrication Technology Department, Advanced Technology and New Materials Research Institute (ATNMRI), City for Scientific Research and Technology Applications (SRTA-City), New Borg El-Arab City, P.O. Box 21934, Alexandria, Egypt.

[2] Departamento de Química Inorgánica, Facultad de Ciencias, Universidad de Granada, 18071 Granada, Spain.

[3] Electronic Materials Department , Advanced Technology and New Materials Research Institute (ATNMRI) , City for Scientific Research and Technology Applications (SRTA-City), New Borg El-Arab City, P.O. Box 21934, Alexandria, Egypt.

[4] Materials Science Department , Institute of Graduate Studies and Research, Alexandria University, 163 Horrya Avenue, P.O. Box 832, Shatby , 21526 Alexandria, Egypt.

Corresponding author:-

***Ch. Hesham Ali Hamad (Hesham Hamad)**

Assistant Researcher , Fabrication Technology Department, Advanced Technology and New Materials Research Institute (ATNMRI), City of Scientific Research and Technological Applications(SRTA-City), Previously "Mubarak City for scientific research and Technology applications (MuCSAT)", New Borg El-Arab City, P.O. Box 21934, Alexandria, Egypt.

Ph.D candidate , Departamento de Química Inorgánica, Facultad de Ciencias, Universidad de Granada, 18071 Granada, Spain.

E-mail: heshamaterials@hotmail.com,

Telephone& faxes

Tel: 0034-631071736 Fax: 002-03-4593414

*** Prof. Dr. Mona Mahmoud Abd El-Latif (Mona Abd El-Latif)**

Dean of Advanced Technology and New Materials Research Institute (ATNMRI), City of Scientific Research and Technological Applications (SRTA-City)

Fabrication Technology Department, Advanced Technology and New Materials Research Institute (ATNMRI), City of Scientific Research and Technological Applications(SRTA-City), Previously "Mubarak City for scientific research and Technology applications (MuCSAT)", **Alexandria, Egypt.**

E-mail address: amona1911@yahoo.com

Prof. Dr. Abd El-Hady Bashir Kashyout (Abd El-Hady Kashyout)

Electronic Materials Department Advanced Technology and New Materials Research Institute (ATNMRI), City of Scientific Research and Technological Applications (SRTA-City), New Borg El-Arab City, P.O. Box 21934, Alexandria, Egypt.

E-mail:hady8@yahoo.com

Associate Prof. Wagih AbdAlim Sadik (Wagih Sadik)

Materials Science Department , Institute of Graduate Studies and Research (IGSR), Alexandria University, 163 Horrya Avenue, P.O. Box 832, Shatby , 21526 Alexandria, Egypt.

E-mail: wagih_sadik@yahoo.com

Associate Prof. Mohamed yousef Feteha (Mohamed Feteha)

Materials Science Department , Institute of Graduate Studies and Research (IGSR), Alexandria University, 163 Horrya Avenue, P.O. Box 832, Shatby , 21526 Alexandria, Egypt.

E-mail: **feteha99@yahoo.com**

Synthesis and characterization of core/shell/shell magnetic ($CoFe_2O_4/SiO_2/TiO_2$) nanocomposite and TiO_2 nanoparticle for photocatalytic activity under UV and visible irradiation.

Hesham Hamad[1,2*], Mona Abd El-Latif [1] Abd El-Hady Kashyout[3], Wagih Sadik[4], Mohamed Feteha[4]

[1] Fabrication Technology Department , Advanced Technology and New Materials Research Institute, City for Scientific Research and Technology Applications (SRTA-City), New Borg El-Arab City, P.O. Box 21934, Alexandria, Egypt.

[2]Departamento de Química Inorgánica, Facultad de Ciencias, Universidad de Granada, 18071 Granada, Spain.

[3]Electronic Materials Department , Advanced Technology and New Materials Research Institute (ATNMRI) , City for Scientific Research and Technology Applications (SRTA-City), New Borg El-Arab City, P.O. Box 21934, Alexandria, Egypt.

[4]Materials Science Department , Institute of Graduate Studies and Research, Alexandria University, 163 Horrya Avenue, P.O. Box 832, Shatby , 21526 Alexandria, Egypt.

Abstract

Magnetic $TiO_2/SiO_2/CoFe_2O_4$ (TSC) composite photocatalytic particles with a core –shell structure with high crystalline anatase TiO_2 shell were synthesized *via* controlled hydrolysis and condensation of titanium isopropoxide. Nano-sized TiO_2 powders were synthesized by sol-gel/hydrothermal route. The prepared TiO_2 and its composite were characterized with XRD, SEM, TEM, FT-IR, VSM, and UV-Vis. The results show that the obtained TSC composite particles were composed of spherical nanoparticles, about 5-8 nm in diameter, with several $CoFe_2O_4$ fine particles as cores and silica as coatings and barrier layers between the magnetic cores and anatase titania shells. TiO_2 nanoparticles with an anatase structure, 6 nm average crystallite size. The photocatalytic activities of the samples were evaluated by the photocatalytic degradation of dichlorophenol-indophenol (DCPIP) dye. The maximum level reached for the degradation of the dye molecule was 95.32 and 87.27% for 3 minute under UV and visible light respectively for mesoporous TiO_2 nanoparticles.

Keywords: Magnetic photocatalyst, Titania, Mesoporous, Sol-gel/Hydrothermal, Co-precipitation, Coating, Core-shell nanostructure, Cobalt ferrite, Photocatalytic activity, Nanocomposites.

1. Introduction

Titanium dioxide (TiO_2) is a photocatalyst widely used for the degradation of organic pollutants in water and wastewater [1],because of its biological and chemical inertness, powerful oxidizing power, high benefit-to-cost ratios, as well as extended stability against photo and chemical corrosion [2–4].TiO_2 can only harvest the spectrum with wavelengths in the near ultraviolet (UV) region ($\lambda < 400$ nm). A serious inherent limitation to the use of TiO_2 is its inefficient exploitation of visible light. Therefore, it is highly desirable to improve the TiO_2nanomaterials in order to increase their optical activity shifting the onset of the response from the UV to the visible region which effective makes up as much as 45% of the total solar energy.

The separation and recovery of suspended small nanostructure TiO_2 particles from treated water is very difficult to operate [5]. Pozzo et al. [6] stated that the cost of the separation might invalidate altogether the claimed energy savings for a solar-induced decontamination process due to the small particle size of the used photocatalyst. This presents a major drawback to the application of the photocatalytic processes for treating wastewaters [7].To solve the problem of separation of photocatalyst, investigators had carried out many researches on immobilizing titania onto various substrates such as glass beads, sand, silica gel, activated carbon fibers and quartz optical fibers [8]. Although this approach provides a solution to the solid–liquid separation problem, slurry-type reactors offer significant advantages over immobilized catalyst-type reactors because of the catalyst surface availability, closer proximity to pollutant and superior mass-transfer properties [9].

Magnetic photocatalysts provide an alternative solution for the problem of response to visible light and separation of photocatalyst. Magnetic photocatalysts consisting of photoactive anatase titania phase and magnetic materials, particularly with core/shell structure, have attracted a variety of attention due to their potential in photodegradation of pollutants along with easy separation from the treated system using an external magnetic field [10-11].Magnetic

nanoparticles combining with catalysts could not only increase the durability of the catalysts but also help to separate and recycle the catalyst particles [12].

Spinel ferrites are an ideal magnetic system for understanding and controlling superparamagnetic properties at the atomic level through chemical manipulation [13]. $CoFe_2O_4$ belongs to the family of Spinels. Spinel cobalt ferrite, $CoFe_2O_4$ is a well known hard magnetic material with very high cubic magnetocrystalline anisotropy, high corecivity, moderate saturation magnetization and their great physical and chemical stability [14].

Magnetic materials might be commercially available or produced by a ceramic process involving high temperature solid state reactions [15] ,sol-gel [16], polyol [17] , Co-precipitation and /or hydrothermal methods [18]and as-prepared magnetic ferrite particles have some disadvantages, for instance asymmetric granule, superparamagnetic properties and weak saturation magnetization, and so forth. To solve these problem, many researchers have prepared high performance spinel ferrite has been reported based on layered double hydroxides (LDHs) [19]. The LDH stabilities were found to vary in the order Mg<Mn<Co ≈ Ni <Zn for M^{II} and Al <Fe for M^{III}. The solubility products of the LDHs vary in the order to Zn <Ni ≈ Co. LDHs can be easily synthesized by coprecipitation of a solution of bivalent and trivalent metal salts with base (usually NaOH or KOH) under laboratory conditions [20].The main advantage of the basic agent titration methods is in the preparation of LDHs with anions other than carbonate. Generally, supersaturation conditions are reached by controlling the pH of the solution[21].

A direct deposition of titanium dioxide onto the surface of magnetic cobalt ferrite particles proved ineffective in producing a stable magnetic photocatalyst, with high levels of photodissolution being observed with these samples[22]. Modifying the properties of one material by coating it with another type of material has been a popular approach widely documented in the literature [23]. The concept of coating one material with another is used to develop a novel magnetic photocatalyst. The photocatalyst is produced by coating a layer of the photoactive material (titanium dioxide) on isolated materials asintermediate on the surface of a magnetic core. The silica layer is also believed to have prevented the iron oxide from acting as an electron-hole recombination centre. This also translates into a higher photoactivity.

This work aims at the preparation and characterization of TiO_2 nanoparticles with small crystal size by sol-gel/ hydrothermal route and hard magnetic composite photocatalyst – cobalt ferrite (magnetic core) / silica (insulated layer) / titania (photoactive shell) (TSC) by direct coating of anatasetitania nanoparticles forming complete coverage using titanium isopropoxide as a titania precursor . The prepared hard magnetic composite photocatalysts can be recovered as well as fluidized by applying an external magnetic field. The microstructure of the as-prepared magnetic photocatalyst was studied by using TEM , SEM, XRD, FTIR, as well as vibrating sample magnetometer (VSM) techniques where UV and solar light was employed to degradation 2.6 dichloroindophenol (DCPIP) dyes. Photocatalytic activity tests reveal that such mesoporousnanotitania and its composite are a superior photocatalysts compared to Degussa TiO_2 (P25).

2. Experimental.

2.1. Materials.

Cobalt nitrate hexahydrate ($[Co(NO_3)_2 \cdot 6\ H_2O]$, 98%) was obtained from BELAMI fine chemicals (Mumbai-India) , Ferrous chloride tetra hydrate ($[FeCl_2.4H_2O]$, 99%) was supplied from ACROS (USA-Belgium), Ferric chloride hexahydrate ($[FeCl_3.6H_2O]$, min. 99%) was obtained from Riedel-de Haen –Sigma Aldrich (Switzerland), Tetraethyl orthosilicate (TEOS) ($Si(OC_2H_5)_4$, ≥ 99 %) was obtained from Merck (Germany), Tetramethylortosilicate (TMOS) , ($Si(OCH_3)_4$, ≥ 98 %) was supplied from Fluka (Switzerland) , Titanium (IV) isopropoxide(TTIP),($Ti\{OCH(CH_3)_2\}_4$, 97%) was obtained from Alfa Asear (Germany),Titanium butoxide ($Ti(OBu)_4$, 97%) was obtained from Aldrich chemicals (Germany), acetylacetone ($CH_3(COCH_3)_2$, 99%) was supplied from Alfa asear (Germany), Urea ($CO(NH_2)_2$, min.99.5%) was supplied from Sisco Research Laboratories (Mumbai-India) , Sodium hydroxide (NaOH, min.99%) was supplied from ADWICEl-Nasr company(Egypt) , Ammonia solution (NH_4OH, Max. 33%) , Hydrochloric acid (HCl,37 %) and Absolute ethanol ($[C_2H_5OH]$, 99.9 %) were obtained from Sigma-Aldrich (E.U) , Nitric Acid (HNO_3 ,65%) was supplied from Pharos (Egypt), 2-Propanol ($(CH_3)_2CHOH$,98%) was obtained from Panreac (E.U), TiO_2 (Degusaa P25 Corporation, Germany) (99.5%) was supplied from Degussa (Germany) and the dye was investigated for photocatlysis was 2,6 dichloro indophenol – sodium salt (DCPIP) ($C_{12}H_6Cl_2NO_2.Na$,97 %) obtained from Sigma (USA). De-ionized water (18.2 MΩ

.cm, TKA-Genpure Instrument) and ultra-pure water for synthesis of titaniawere used in all the synthesis experiments. Molecularstructure of DCPIP dye as shown in Fig. 1.

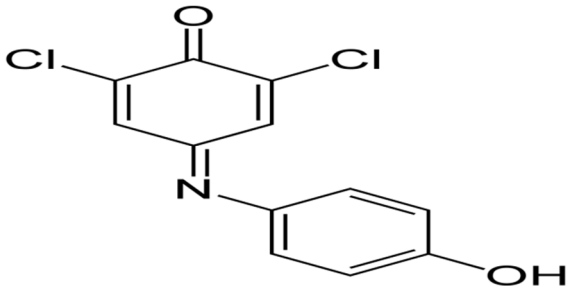

Figure 1: Molecular Structure of DCPIP dye.

2.2. Synthesis of Highly Active TiO_2 Nanoparticles.

In a typical preparation procedure, Titanium butoxide ($Ti(OBu)_4$) wasused as a titanium precursor , an acetyl acetone (acac) complexing agent was used to control the rate of hydrolysis and condensation reaction of the precursor. De- ionized water as a solvent (18.2 MΩ.cm, TKA-Genpure) .10 % Nitric acid used as a catalyst was then added to the mixture under stirring condition. The molar ratios of the ingredients were as follows: Titanium precursor / acac / 10%HNO_3 / De-ionized water = 1:1:3:20. The pH values of resulting solutions were 3. The final solution was stirred for 6 hrs at room temperature. The resulting sol was placed in 80 ml Teflon lined stainless steel autoclave, which was then placed in an oven for hydrothermal treatment at 170 ^oC for 72 hrs.This sample is denoted as 4C.

2.3. Synthesis of Core/Shell/Shell structured magnetic nanocomposite($CoFe_2O_4/SiO_2/TiO_2$).

A magnetic photocatalyst was prepared by coating of $CoFe_2O_4$ as magnetic core with an insulating silicon dioxide (SiO_2) layer and photocatalytic properties of the outer titanium dioxide shell. The overall procedure for synthesizing Core/Shell/Shell structured Magnetic nanocomposite ($CoFe_2O_4/SiO_2/TiO_2$) was synthesized by three steps is presented in Figure 2.

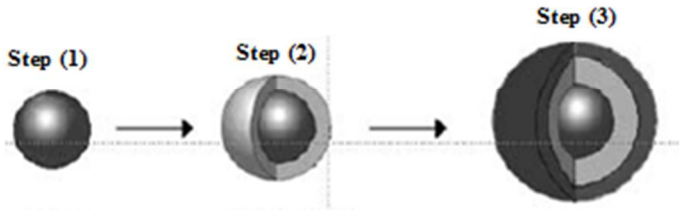

Figure 2: Overall procedure for the synthesis of core-shell-shell $CoFe_2O_4$ / SiO_2 / TiO_2 nanocomposite.

2.3.1. Synthesis of $CoFe_2O_4$ LDHs nanoparticles by Co-precipitation method.

The magnetic core Cobalt spinel ferrite nanoparticles were prepared from a Co-Fe LDH precursor using co-precipitation method. A typical synthesis is as follows: an aqueous solution of $Co(NO_3)_2.6H_2O$, $FeCl_2.4H_2O$and $FeCl_3.6H_2O$with molar ratio of Co^{2+}: Fe^{2+}: Fe^{3+} = 2:1:2 were dissolved in de-ionized water. A NaOH aqueous solution (1.5mol/L) was added dropwise into above solution under N_2 atmosphere until the pH reached 7.0 to ensure complete precipitation. The resultant slurry was removed from three neck flask and aged at 40^{o}C for 4 hrs to increase crystallinity. The final precipitate was washed with deionized water and ethanol and filtered by vacuum pump (Barnant, Model 400-3912, USA), and dried at 50^{o}C under vacuum (Barnstead Lab-Line, Model 3618-6CE, USA) for 24 hrs. This sample is denoted as 1C. Such obtained LDHs precursor was then calcined in muffle (Barnstead International, Model F4800, USA) at 900^{o}C for 2 h resulting in the $CoFe_2O_4$ magnetic core (sample 1CM1) .

2.3.2. Synthesis of silica coated cobalt ferrite nanoparticles ($CoFe_2O_4$ / SiO_2).

Coating of cobalt ferrite with silica layer was carried out by using ferrites as seeds.The $CoFe_2O_4$/SiO_2 particles were obtained using the conventional sol–gel process. In detailed, 0.5 g $CoFe_2O_4$ particles were dispersed in 230 ml isopropanol and sonicated for 25 min in an ultrasonic cleaning bath (Ultrasons, Spain). 6 ml of tetraethyl orthosilicate (TEOS) or tetramethylortho silicate (TMOS) were added to the sonicated solution at the pH value adjusted

to 10.5 with NH_4OH. The resultant solution was vigorously stirred at room temperature for 10 hrs. The resultant was washed with deionized water followed by ethanol, and dried at 115 ^oC (Nabertherm, Model TR60, Germany) for 24 h giving the silica modified $CoFe_2O_4$ sample and denoted as SC for TEOS and SC2 for TMOS sources.

2.3.3. Synthesis of core/ shell/ shell ($CoFe_2O_4$ / SiO_2 / TiO_2) nanocomposite.

The shell anatase TiO_2nanocrystals was directly coated on SC particles via sol–gel hydrolysis precipitation of titanium isopropoxide (TTIP) followed by calcination treatment. A certain amount of SC particles were dispersed in 200 ml ultra-pure water (18.2 MΩ. cm , TKA-Genpure) and stirred for 30 min. 5 ml of TTIP were added dropwise into above mixture followed by addition of 3.6 g urea. The resultant suspension was stirred for 1 h at room temperature (Selecta, Model Agiamatic-ND, Spain), and finally heated to 120 ^oC for the next 24 h under stirring vigorously. The obtained sample was washed with deionized water followed by ethanol, and dried at 70^oC for 2 days in a vacuum. The resultant sample was denoted as TSC. A proper amount of TSC was heated at 300 ^oC for 1 h giving the sample TSC-300.

2.4. Sample Characterization.

2.4.1. X-ray diffraction (XRD)

Crystal phases and crystallie size of as prepared samples are obtained by X-ray diffraction using Shimadzu- XRD- 7000 Diffractometer (Japan) operating at room temperature with Cu (Kα) radiations of wavelength (λ= 1.5406 Å), generated at 30 Kv – 30 mA. The 2θ range for all samples was in the range of scan step size $10^o < 2\theta > 80^o$with Scan speed of 4^o/s. The crystallite size was calculated using Scherrer equation (equation 1) [24].

$$L = K \lambda / (\beta \cos \theta) \qquad (1)$$

Where L is the crystallite size (Å), λ is the wavelength of the X-ray radiation (Å), K is usually taken as 0.89, β is the line width at half-maximum height (radians) and θ is the diffraction angle (degree). The average crystal size was estimated by applying the Scherrer equation to the apparent full width at half maximum intensity (FWHM) of the (101) peak of anatase TiO_2 or the (110) peak of rutile TiO_2 [25].The phase composition of the samples can be calculated from the equation 2 [26].

$$X_R = 1 - (1/ (1+1.26(I_R/I_A)) \qquad (2)$$

Where X_R is the weight fraction of rutile in the mixture, and I_R and I_A are the relative intensities of the strongest diffraction peaks rutile and anatase , respectively.

2.4.2. Morphological Characterization.

2.4.2.1. Scanning Electron Microscopy (SEM).

The prepared samples have examined with scanning electron microscope (JEOL, Model JSM 6360LA, Japan).

2.4.2.2. Transmission Electron Microscopy (TEM).

Crystallite sizes and shapes of the prepared samples were confirmed by transmission electron microscopy which was performed on a TEM (JEOLJEM1230,Japan) with maximum magnification 600k×and resolution 0.2 nm. Samples for TEM measurements were suspended in ethanol and ultrasonically dispersed.

2.4.3. Fourier Transform Infrared Spectroscopy (FT-IR).

FT-IR spectra of titanium dioxide were recorded using FTIR spectrophotometer Shimadzu-8400 S (Japan), IR transmission spectra were taken in the range from 400to 4000 cm^{-1} with scan rate was 2 cm^{-1} s^{-1}.

2.4.4. Vibrating sample Magnetometer (VSM).

VSM can generate a magnetic field as high as 20 kOe and can provide magnetic moment sensitivity up to 1μemu. The magnetic measuring mechanism is a VSM, which belongs to an inductive technique and can be operated from room temperature in a Lake Shore-7410 vibrating sample magnetometer**.**

2.4.5. UV/Vis Spectroscopy.

UV/Vis spectrophotometer is used to monitor the electronic energy level of a molecule. After preparation of samples, the wavelength and absorbance is measured using ultraviolet-visible spectrophotometer (Spectro UV-Vis Double Beam PC Scanning , Labomed, Inc).

2.5. Measurement of Photocatalytic Activity.

The photocatalytic performance of the as prepared $TiO_2$and its composite were investigated by using the photocatalytic decomposition of dichlorophenol-indophenol (DCPIP) in aqueous solution under ultraviolet and visible irradiation. The photocatalytic degradation of dichlorophenol-indophenol dye (DCPIP) were performed in a slurry reactor (Figure 3a) at constant room temperature (25±1^{o}C) .The photocatalytic degradation was carried out at 1g/L Catalyst, 1× 10^{-4} M for dye solution and natural pH, which was 6.7. The slurry reactor comprised of a glass container (1 liter). The contents (DCPIP dye and catalyst) were maintained as a suspension by means of a magnetic stirrer (Selecta, Model Agiamatic-ND, Spain). Then, dry air was fed into the solution with rate 4L/min. A tubular low pressure mercury vapor source (total rating 43 watts, total UV output at 254 nm 13.4 watts, length 120 cm, VALBER LOURMAT , Germany) was used to irradiate the solution which was located 10 cm from the surface of the source . The total intensity reaching the slurry solutions measured using a UVX radiometer (UV products Ltd., Cambridge) equipped with a sensor with peak sensitivity was 4mWcm^{-2}. The local volumetric rate of energy reaching the solutions was 2.1μ Einstein's^{-1} L^{-1}at 254 nm. The Photocatalytic activities of $CoFe_2O_4$ /SiO_2/ TiO_2were evaluated in terms of the degradation of DCPIP as a model using a visible irradiation. The Photocatalytic reactor included three parts (Figure 3b): 1000 ml glass beaker, stirrer and 500 W Xenon lamp (Houras Scientific Co., Egypt)was used as a visible light source. The distance between the light and the liquid reaction were fixed at 10 cm and lamp was cooled with air. The ambient temperature is maintained during the photocatalytic reaction because of good ventilation. At the given time intervals, a sample of 5 ml were taken from the mixture then filtered through 0.2 μm Whatmann filter to remove photocatalysts. The concentration of the filtrate was analyzed by checking the absorbance at 600 nm with UV-Visible spectrophotometer. The photoactivity of the prepared particles was compared to that of the commercially available photocatalyst, Degussa P25(TiO_2, Degussa P25, primary particle diameter of 18.2 nm , specific surface area 50±15 m^{2}g^{-1} and a crystal distribution of 75.3 % anatase and 24.7% rutile), under the same conditions. Total reaction time was in all cases was 45 minutes.

The degree of DCPIP decolorization could be calculated according to the equation 3:

$$\text{Degradation rate} = C_o - C / C_o \times 100\% = A_o - A / A_o \times 100\% \qquad (3)$$

Where C_o = initial concentration of dye solution, C = concentration of dye solution after photoirradiation at time t. $A_o$is the value of absorbance of dye aqueous solution after adsorption in the dark, and A is the value of absorbance of dye aqueous solution after reaction.

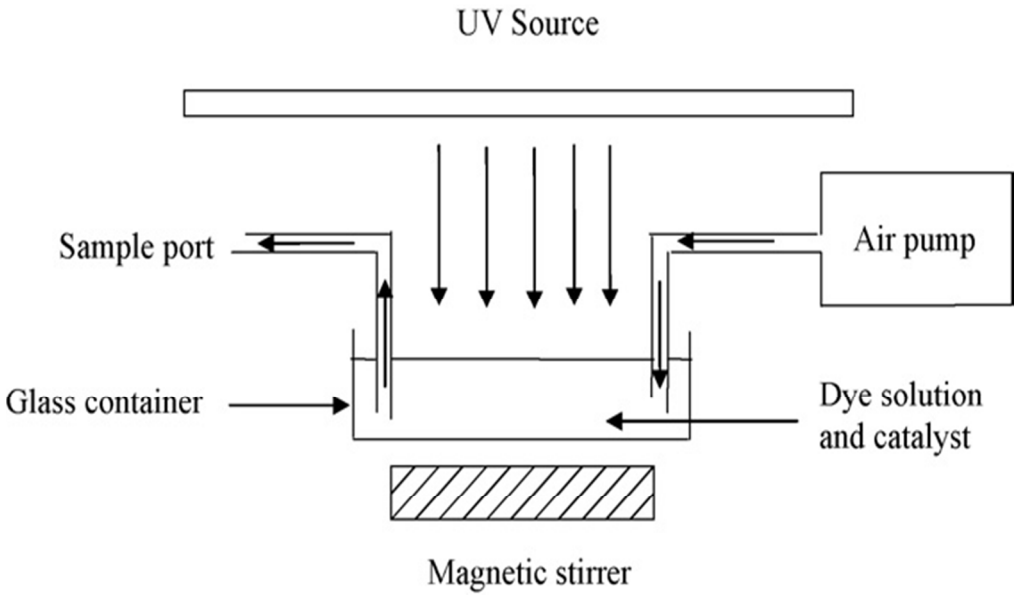

(a)

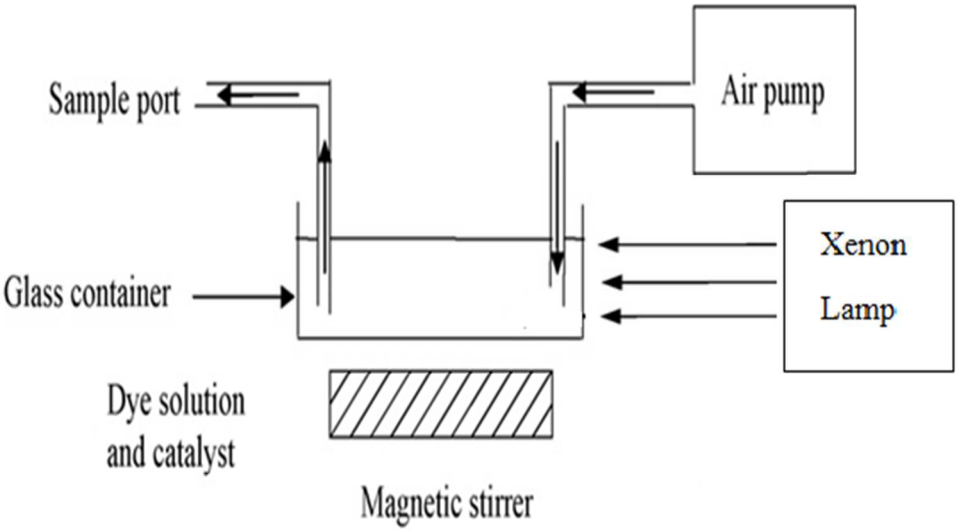

(b)

Fig.3: Schematic diagram of bench slurry photoreactor a) UV and b) Visible type.

3. Results and Discussion.

3.1. X-Ray Diffraction Studies.

Figure4 shows the XRD patterns of as prepared TiO_2 and magnetic nanocomposite that indicate $CoFe_2O_4$ (1C), $CoFe_2O_4$ -900 (1CM1),SC, SC2, TSC, TSC-300, as prepared TiO_2(4C) and Degussa P25. In figure (5.a), The as prepared $CoFe_2O_4$ structure belongs to the inverse spinel group with the general formula A (B_2) O_4. The peaks appeared at 18.2°, 30.0°, 35.4°, 37.2°, 43.47°, 57.1° and 62.72° are attributed to (111), (220), (311), (222), (400) , (511) and (440) reflections of the spinel phase of $CoFe_2O_4$[10]**.**The basic characteristic peak did not appear which indicated that the crystallization of the precursor was incomplete after drying with a very small crystal size according to Scherer's formula using (JCPDS, card No. 003-0864) (Table 1) with a space group of Fd3m, and this amorphous nature disappears and the diffraction peak of (311) crystal plane appears. In addition, the peak shape in (Figure 4b) was relatively narrow and high, which indicates that the crystal grew up with increasing temperature to 900^oC, and the crystallization was complete indicating that the peak intensity increased with increasing calcinations temperature and that crystalline phase of the prepared $CoFe_2O_4$ is stable during heat treatment. By controlling the temperature of heat treatment, the size of these nanoparticles can be varied from 11.5 to 87.4 nm in particle size analyzer. The XRD pattern for SC from precursor TEOS (Figure 4 c) remains almost identical with that of $CoFe_2O_4$ except a broad weak peak at 2θ ~23^o (*JCPDS*, card number 27-1402), indicating that the silica shell is amorphous and the crystallinity of the magnetic nanoparticle is largely retained after the coating, as in the case often occurred for silica-coated spinel ferrite. The peaks of SiO_2 are not observed because they are mainly amorphous, and this amorphous silica layer would provide an intermediate layer preventing the direct contact for eliminating the photodissolution of magnetic cores due to the small ionic radius (0.041 nm) of Si^{4+} in comparison of ionic radius (0.074 nm) of Ti^{4+} ions indicated that not make substitution [27]. The crystal size of $CoFe_2O_4$ in SC is decreased in comparison of $CoFe_2O_4$-900 (Table 1). For sample SC2 from precursor TMOS (Fig.4d), It was found that there is a wide broad amorphous with the maximum peak between 20^o and 30^o besides some peaks from $CoFe_2O_4$. Silica precursors used to make a sol-gel, however, silicon alkoxides such as tetraethoxyorthosilicate (TEOS) and tetramethoxyorthosilicate (TMOS) are desirable because they contribute to better purity and control of colloid formation and growth. TMOS will

hydrolyze very rapidly but in doing so will produce toxic methanol and is time limited in the condensation step. TEOS hydrolyzes slower but produces ethanol which is less toxic than methanol to the face and lungs so is often the precursor of choice [28].The presence of silica in TiO_2 particles could effectively suppress the formation of the rutile phase, the growth of the titanium dioxide crystals, and the reduction of surface areas during the calcinations process[29]. The two expected phase ($CoFe_2O_4$ and TiO_2 anatase) were identified for the samples TSC and TSC-300 in Figure 4 e and f. The pattern shows (101), (220), (311), (222), and (422) diffraction peaks related to crystal structure of anatase phase with little rutile for TiO_2 and spinel phase for $CoFe_2O_4$ without brookite (Table1)(JCPDS, Card No. 021-1272,021-1276 for anatase and rutile, respectively) **.**For fig. 4e, the presence of rutile TiO_2 phase was not detected and no peaks related to pure iron or cobalt phases such as hematite or cobalt oxide. The molar fraction of anatase to rutile (X_A), calculated according to equation (2) was estimated as 84.1%. The crystal size of TiO_2 decreases when Fe^{3+} incorporated into the crystal of TiO_2 [30].It shows evidently weakened line intensities of $CoFe_2O_4$, and the amorphous SiO_2 feature at failed 2θ ~23^{o}to be detected instead with two broad ones at 25.48 and 48.18 ascribing to the characteristic (101) and (200) lines of anatase phase, implying that the very small TiO_2 particles may enwrap up the SC particles. The intensity of spinel phase of $CoFe_2O_4$is decrease in comparison to SC. The radius of Fe^{3+} (0.64˚A) is similar to that of Ti^{4+} (0.68˚A). In the case of samples containing iron, no significant characteristic peaks for iron oxide were detected, which suggested that no significant iron segregation was produced in the samples. There are two reasons responsible for this result. One possible reason is that the Fe^{3+} content in the Fe–TiO_2 samples is below the detection limit of this technique. Another is that all Fe^{3+} ions might substitute Ti^{4+} ions and insert into the crystal lattice of TiO_2 because the radii of Ti^{4+} and Fe^{3+} ions are very similar [31]. The crystallite size calculated after the heat-treatment is 6.2 nm. The most intense peak at $2\theta = 25.2^{\circ}$ among the anatase titania peaks is detectable in the XRD patterns; the spinel phase of $CoFe_2O_4$ remains essentially unchanged during heat treatment, It depicts slightly enhanced (101) line due to slightly enhanced crystallinity of anatase and evidently increased lines for $CoFe_2O_4$ compared to raw TSC. It is still broad and weak because of the low titania loading percent and much smaller crystal size of titania. It is concluded that the incorporation of iron in these catalysts does not catalyse the anatase to rutile phase transformation, at least at the temperatures at which these catalysts are calcined. In case of mesoporous TiO_2 without calcination (Fig.4g), the broaden

diffraction peak of anatase is observed and the crystal size with about 6 nm and the most phase is anatase without rutile (Table1). The main peaks corresponding to standard anatase TiO_2 including (101), (004), (200), (105), (201), (204), (116), and (220)are observed. Degussa P-25 (Fig. 4h) contains about 24.68% of the rutile phase. The diffraction peak of P25 has anatase and rutile structure, and its crystal size is approximately 18 nm with anatase and rutile phase.

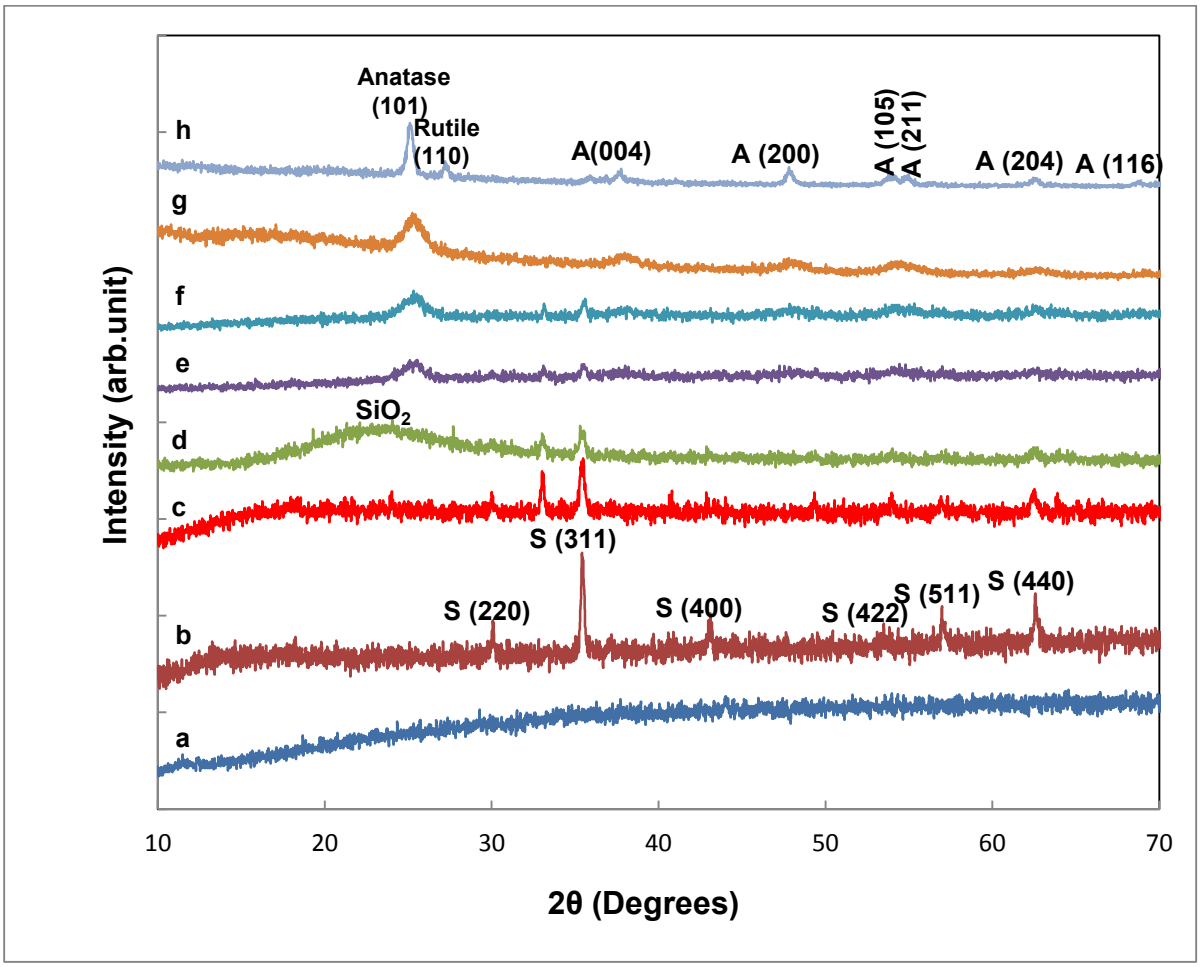

Figure 4 : Wide angle XRD patterns of ; a) 1C , b) 1CM1, c) SC, d) SC2, e) TSC, f) TSC-300 , g) 4C, h) and Degussa p-25. A: Anatase , S: Spinel.

Table 1: Crystallite size from XRD for the prepared sample

Sample	Crystallite Size of $CoFe_2O_4$ (nm)	Crystal Size of Anatase TiO_2 (nm)	Percent of Anatase (%)
1C	------	------	-----
1CM1	37.57	------	-----
SC	22.61	------	----
SC2	14.51	------	----
TSC	-----	5.8	84.1
TSC-300	------	6.2	91.9
4C	-----	6.0	100
P-25	-----	18.2	75.3

3.2. Morphology Studies and formation mechanisms.

3.2.1. Scanning Electron Microscopy Studies.

The structural morphology of nanoparticles was investigated through SEM. Figure 5a shows the SEM images of $CoFe_2O_4$as calcined at 900 ^oC that prepared by co-precipitation method. The images have uniform spherical structure morphology with a narrow size distribution of particles. Different surface morphologies due to the silica coating in sample SC (TEOS precursor) are visible in Fig.5b. The cobalt ferrite particles are agglomerated after coating with silica because of the magnetic attraction between cobalt ferrite particles and the necking between silica layers [32].Silica coated cobalt ferrite from TMOS (SC2) is shown in Figure 5c indicated that increase percentage of silica and non homogeneity of coating on the On the contrary for silica coated cobalt ferrite from TEOS (SC). The SEM micrographs of the titania coated silica coated cobalt ferrite particles are presented in Figure 5d. These results indicate the heterogeneous nucleation of TiO_2 nanoparticles on silica coated $CoFe_2O_4$ nanoparticles, with increasing surface roughness; this effect is synergistic, since it is not observed in pure materials ($CoFe_2O_4$ and TiO_2). It is also important for the photocatalytic activity of the materials, since their efficiency is directly related to the photocatalyst. Another interesting property is the low particle size of coated titania in the

as-synthesized nanocomposites.Figure 5e shows the affect of heat treatment on TSC (TSC-300) by SEM .It shows that increase in particle size after heat treatment leads to decrease of photoactivity. The morphology of synthesized material and Degussa P-25 has spherical shape as shown in Fig.5 f and g. The mesoporous TiO_2 probably arises from the aggregation of nanocrystalline TiO_2 particles. Further hydrolysis and condensation of titanium precursors lead to the growth of larger TiO_2 nanoparticles, which are slowly aggregated to one another. Similar aggregation of nanoparticles leading to mesoporous sphere also studied by Yang et al [33].

Formation of coating particles exist in solution while other particles are being deposited, the existence of the seed particles creates a new scenario for the precipitation and formation of the new phase. As the new phase precipitates, three processes may be occurred. Firstly, the reactants can absorb on the surface of the seed particles, and the new phase can directly precipitate on the seed particles. Secondly, the new precipitated phase can originate as nanosized particles, precipitated separately in solutions (homogeneous precipitation), which then interact with and adhere to the surface of the particles. Finally, the new phase may form with minimal interaction with the seed particles. When this occurs, the end result is a mixed system in which the seed particles and the newly precipitated phase coexist as separate phases [34].

Energy dispersive X-ray results confirmed of transition metal atoms in each material according to the nominal stoichiometry as shown in Table 3. Only three kinds of elements, Co, Fe and O are detected and their mass ratios are corresponding to $CoFe_2O_4$ chemical composition. These results revealed the sustained spinel structure of the $CoFe_2O_4$ crystal for calcinations temperature at 900 ^oC .The atomic ratio of Fe: Co for the entire calcined sample is maintained at ~ 2:1. The EDAX results showed that all products did not contain the element of Na. This result indicated that the Na cations did not take part in the reaction. The EDAX spectrum image from the intermediate silica layer coated cobalt ferrite magnetic core showing the presence of cobalt, iron, silicon and oxygen. Chemical analysis indicates the sample contains atomic percent of iron greater than from $CoFe_2O_4$. The EDX spectrum of the external shell shows a strong Si signal at 1.8 keV, confirming that the external shell is composed of SiO_2. A strong Fe, Co peak is observed at 6.4 and 7.0 keV with weight percentage 38.15 and 8.65, respectively, in addition to Si peaks. It can be seen that the EDAX spectrum image taken from the cobalt ferrite magnetic core region shows the presence of cobalt, iron, silicon, titanium and oxygen. The EDAX

spectrum of the external shell shows a strong Ti signal at 4.5 eV with atomic percentage 36.39 %, confirming that the external shell is principally composed of TiO_2. The X-ray beam is positioned on the inner shell, in addition to the Ti signal, indicating that the intermediate shell layer is composed of SiO_2. Since the particles are spherical, TiO_2 shell is also crossed by the electron beam, which leads to the presence of a Ti signal. The EDAX spectrum shows that decrease at intensity of silicon with atomic percent less than 2 % in comparison of SC. In the EDAX spectrum of the core, a weak Fe peak is observed with atomic percent less than 5 %, in addition to the Ti and Si peaks. The EDAX spectrum of the external shell shows a strong Ti signal with atomic percentage 35.73 %, confirming that the external shell is principally composed of TiO_2. The X-ray beam is positioned on the inner shell, the EDAX spectrum of Si signal at 1.8 eV disappears, in addition to the Ti signal. TiO_2 shell is also crossed by the electron beam, which leads to the presence of a Ti signal. In the EDX spectrum of the core, a weak Fe peak is observed with atomic percent around 5 %, in addition to the Ti and Si peaks. No vague peaks associated with other crystal structures were observed. The as-prepared sample was expected to contain only Ti and O elements. The EDS spectrum of the titania shows a strong Ti signal at 4.5 eV with atomic percentage of 29.35 %, confirming that the external shell is principally composed of TiO_2 (Figure already in supplementary figures)

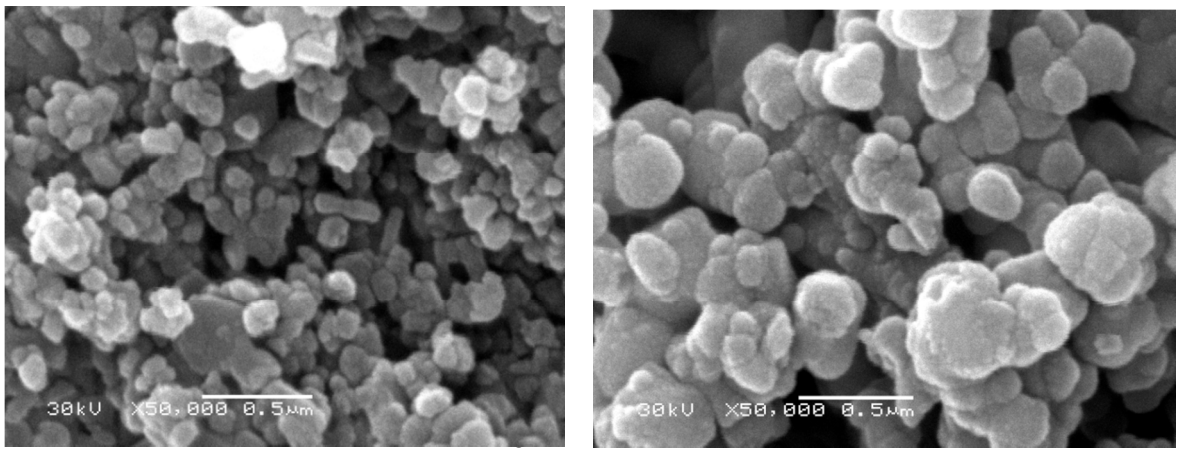

(a) (b)

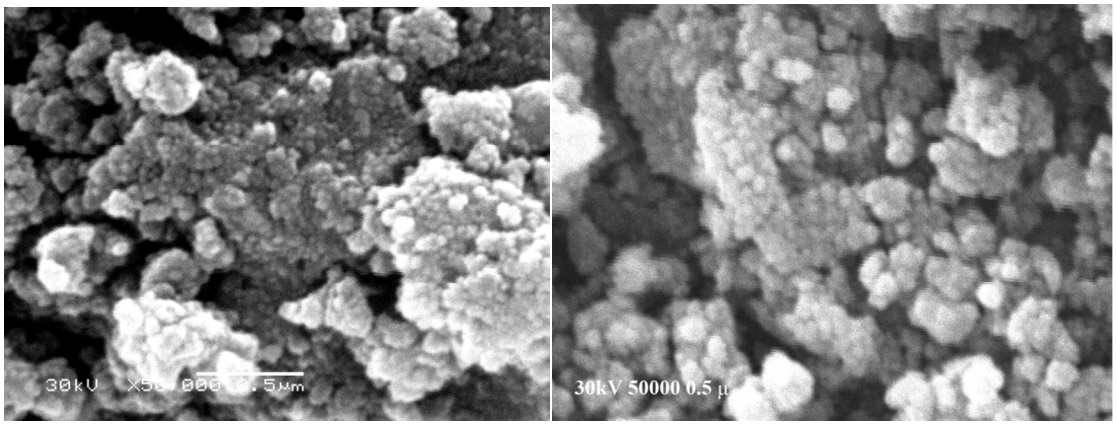

(c) (d)

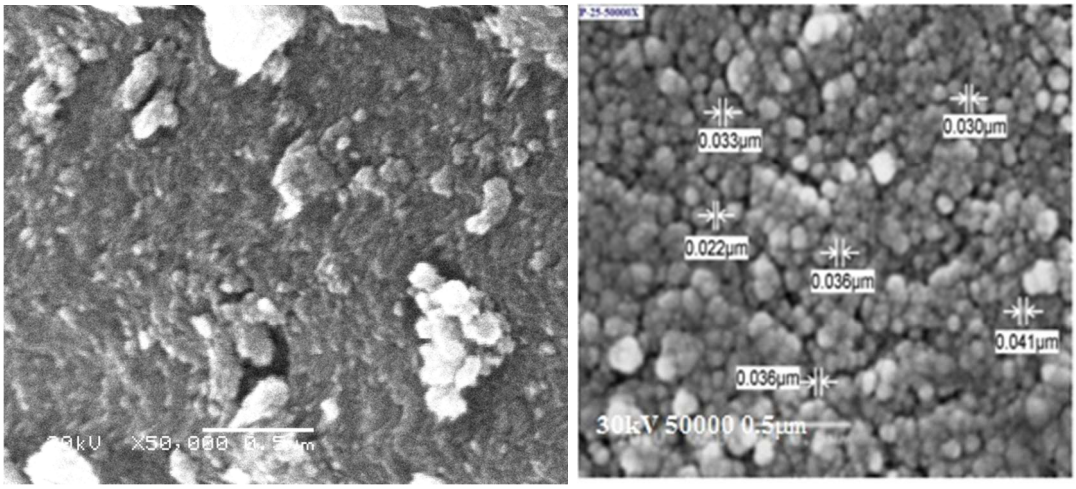

(e) (f)

Figure 5: SEM image of as calcined $CoFe_2O_4$ (a), SC (b) , TSC (c),TSC-300 (d), 4C (e), f) and Degussa P-25.

3.2. 2. Transmission Electron Microscopy Studies.

Figure 6a depicts the typical TEM images of cubic cobalt ferrite nanoparticles calcined at 900^{o}C with average particle size 50 nm with many layers indicated on LDHs. In figure 6 b silica thin layer were obviously coated calcined cobalt ferrite. This indicated that there is a significant increase for specific surface area when adding small amount of SiO_2. The TEM of TSC sample shows a relatively rough but still coherent coating with small black dots decorating the silica ferrite surface thickness with near spherical TiO_2 particles in diameter 2.8-5.7 nm over the lightly

SC particles. In general, free titania particles are rarely seen in the present TSC samples upon TEM analysis due to the existence of an adhesion SiO_2 layer, though a little SiO_2 particles may be mixed with the outside TiO_2 particles. It can be seen that titania layer has a great influence on the photocatalytic activity of the nanocomposites as shown in Figure 6c. This clearly shows the effect of the improved crystallinity after the heat-treatment. As shown in Figure 6d, the sample with 2.8-5.7 nm thick titania shell is less than the thickness in calcinedtitania at 300 ^{o}C (6-49nm). The increase of the thickness of the titania layer leads to a decrease in the photocatalytic activity, consistent with the relatively smaller surface area of thicker titania layers when the total amount of titania is kept constant. In sum, a magnetic nanocomposite TSC was obtained and having core (magnetic ferrite) – tentative intermediate layer (silica) – shell (titania) structure, which can be used as a photocatalyst for organic degradation with potential magnetic separation ability. Figure 6e shows the TEM images of mesoporous TiO_2 nanoparticles (with average crystallite size of about 21 nm as determined by XRD) with particles of sizes 5-8 nm. Most of the particles appear spherical in shape are also present as shown in the TEM images. The mesoporous TiO_2 probably arises from the aggregation of nanocrystalline TiO_2 particles.

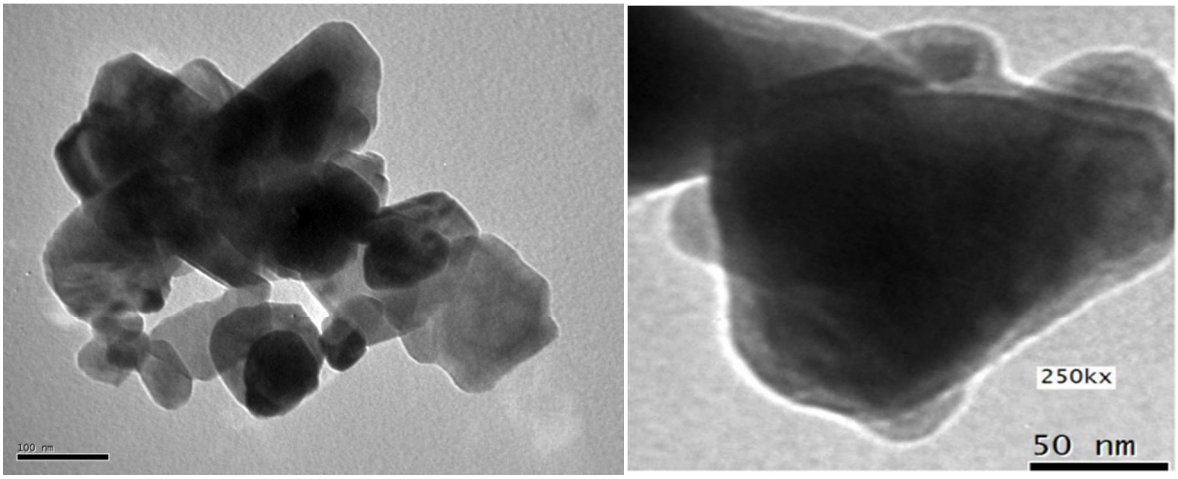

(a) (b)

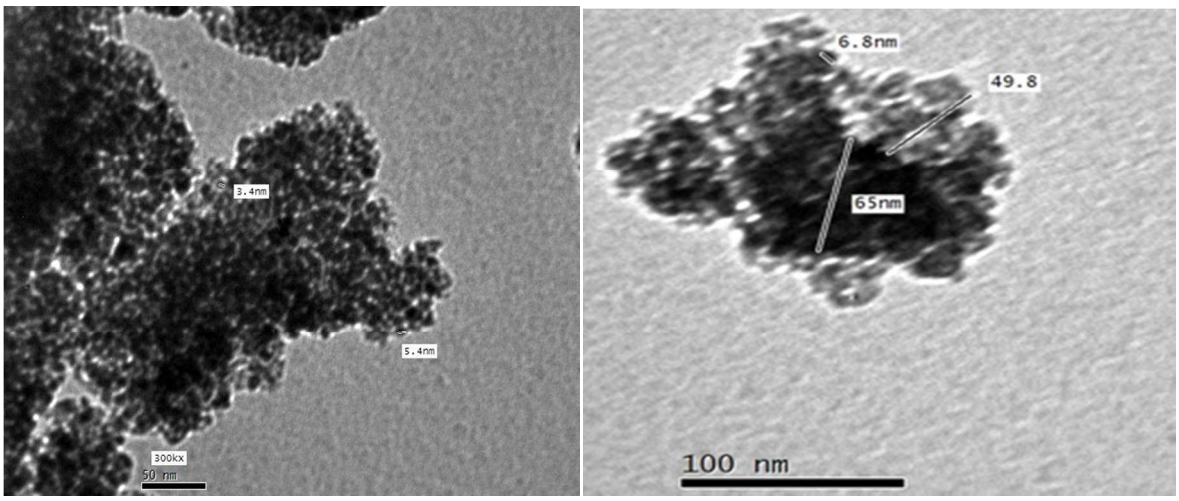

(c) (d)

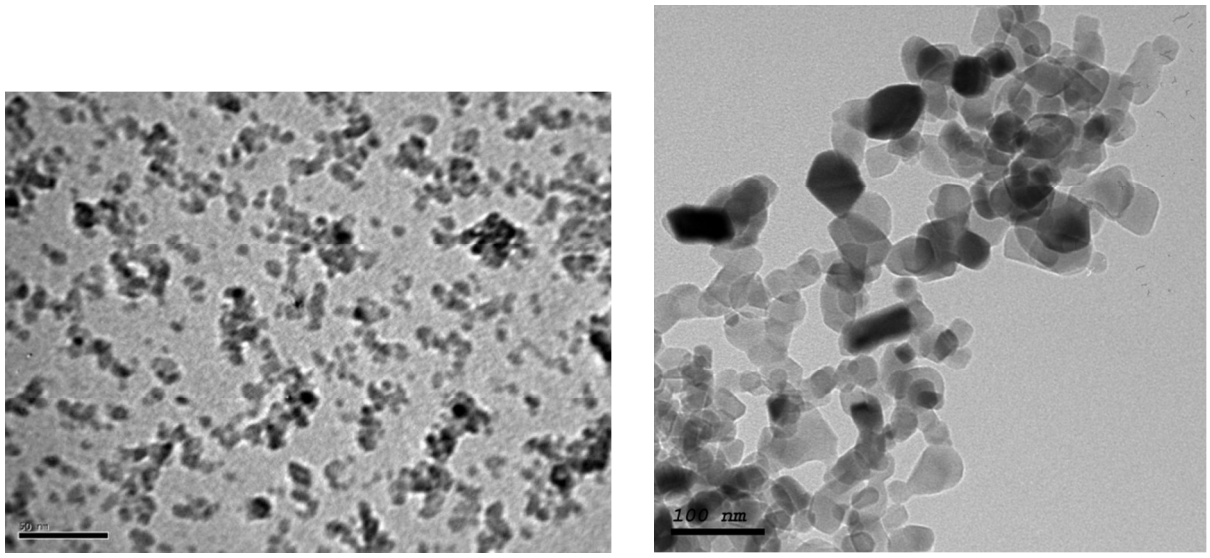

(e) (f)

Figure 6: TEM image of as calcined $CoFe_2O_4$ (a), SC (b) , TSC (c),TSC-300 (d), 4C (e), f) and Degussa P-25.

3.3. FT-IR Studies.

Figure 7 depicts the FTIR spectra of the nanocomposites. The absorption band at ~3440 and at 1627 cm^{-1} are observed in all spectra and can be ascribed to the stretching mode of the surface hydroxyl groups and bands of water, respectively.This surface hydroxylation is advantageous for the photocatalytic activity of TiO_2 because it provides higher capacity for oxygen adsorption

[35]. The characteristic of nitrate bands at 1377 cm^{-1} are intense in the spectrum of as prepared cobalt ferrite (1C) as shown in Fig. 7a. A band centered at 1383 cm^{-1}, indicates the presence of NO_3^- ions (N–O stretching vibrations) [36]and/or C–H group compounds (C–H bending vibrations) in the gel[37].From Figure7 b, the broad band with low intensity at 3400 cm^{-1} confirms the presence of hydroxyl group on iron oxide surface. Bands at about 561cm^{-1} corresponds to Fe–O vibration modes. At the same time metal-oxide vibration band characteristic of cobalt ferrite (587cm^{-1}) increases, corroborating the spinel structure characteristics of cobalt ferrite, assigned the high-frequency bands to the tetrahedral group [38]. For sample SC , The band for Si–O–Si stretching vibration at range of 1114 cm^{-1} of the SiO_4 tetrahedron was further broadened while that for the Si–O–Si or O–Si–O bending mode at 465.70 cm^{-1} was much weaker, which corresponded to a rearrangement process of the silica network [39] as shown in Figure 7c . The presence of Si–O–Si bond in FT-IR is caused by the formation of SiO_2 in the samples. However, this phase is not detected using XRD. The absence of this phase indicates that SiO_2 is occurred in amorphous phase and it is in agreement with the reported result [40]. The high intense peaks than $CoFe_2O_4$ peak were assigned to the OH bending and stretching of water at 1635 and 3441 cm^{-1}, respectively. The Si–O–Fe bond was also evident by the presence of another band at 576.68 cm^{-1}, which is associated with the Fe–O stretching in Si–O–Fe bonds. The band due to Fe–O (~ 600 cm^{-1}) is greatly weak compared with that in $CoFe_2O_4$ probably due to the modification of SiO_2 onto $CoFe_2O_4$[41].Figure 7 d shows that a band at 597.89 cm^{-1} was observed in the TSC sample that can be attributed to the Ti–O–Ti vibration [42] compared with that in the SC sample (Figure 7c) , the intensity of the two absorption bands around (1630,3400 cm^{-1})in TSC is much weaker. This indicates that the introduction of coated TiO_2 makes the catalyst possess more surface hydroxyl groups than coated SiO_2. It is generally admitted that titania strongly retains adsorbed undissociated water due to the strong Lewis acidity of the co-ordinatively unsaturated Ti^{4+} surface sites [42]. The hydroxyl groups will play an important role in the photocatalytic reaction because they can capture the photoinduced holes and then form hydroxyl radicals with provides higher capacity for oxygen adsorption. The IR bands of TSC from 910 to 960 $cm^{-1}$and stretching vibration at 1114.78 cm^{-1} may be attributed to the formation of the Ti–O–Si and Si–O–Si bond respectively were not observed due to the silica content was small [43]. The absorption band at 3440 cm^{-1} observed in all spectra can be ascribed to the stretching mode of the surface hydroxyl groups. Since TiO_2

crystallites are very small, the local environment of Ti– OH bonding was not homogeneous .In summary, FT-IR spectra confirmed that prepared composite nanoparticles might be chemically bonded materials. In Figure 7e , The weak band at 1224.71 and 2352.99 cm^{-1} were attributed to C-O and ν_{OH} stretching mode of interacting hydroxyl groups (i.e., involved in hydrogen bonds) and the symmetric and asymmetric$_{\nu OH}$ modes of molecular water coordinated to Ti^{4+}cations[44] , respectively, that not found in TSC (Figure 7 d). The obviously broadened band in the range 800– 450 cm^{-1} is detected, implying the existence of Ti–O stretching[45]due to the TiO_2 coating on SC particles .The band at 597.89 cm^{-1} is TSC are shifted to 466.74 cm^{-1} in TSC-300 (Figure 7e)which attributed to Ti-O-Ti band corresponding to Chhor et al.[46] was also observed for Ti-O-Ti band at 495 – 436 cm^{-1}. The weak band at 2349.14cm^{-1} attributed to $_{\nu OH}$ mode of interacting hydroxyl groups (i.e., involved in hydrogen bonds [43] as shown in figure 7 f,g. The intensity band at 1394 cm^{-1}istertiary C-OH bending (Figure 7f), It is bonded to Ti from the presence of alkyl groups that can ascribed to the characteristic frequencies of residual organics species. The broad peak at 490 cm^{-1} is attributed to $\nu_{Ti\ -O-\ Ti}$ stretching vibration in the anatase phase that indicated characteristic strong absorbance of TiO_2 due to Ti-O stretching Ti-O-Ti bridge stretching vibration or bending vibration [44].

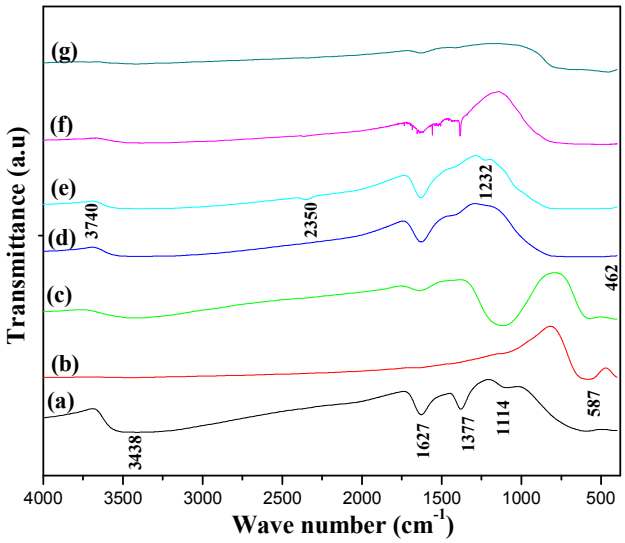

Figure 7: FT-IR spectra for ; a) 1C, b)1CM1, c)SC, d) TSC, e)TSC-300, f) 4C , g) and DegussaP-25 .

3.4. Magnetization Studies.

The magnetic properties of as-prepared $CoFe_2O_4$ and itsnanocomposite were investigated with a quantum magnetometer by a VSM (vibrating sample magnetometer) at 300 K ($T > T_B$) with a maximum applied field up to 20 kOe are presented in Figure 8 and Table 3. The saturation magnetization (M_s) values of about 13.6 and 70.628 emu/g indicative of strong soft magnetic propertiesfor $CoFe_2O_4$ as prepared and calcined at 900^{o}C, respectively as shown in Figure 8 and Table 2. The saturation magnetization and remenant magnetization increased with increasing heat-treatment temperatures. This happened because of the incomplete crystallization and small particle size after treating at low temperatures. Meanwhile, other factors such as the large proportion of surface atoms, the unsaturated ligand, and the strong thermal disturbance characteristics could play a role [19]. Therefore, the magnetic structure of the crystal was unstable and disorder and the magnetic moment cannot be easily kept to be consistent with the external field. In addition, because the powder surface had a non-magnetic layer, and the proportion of the layer decreased with increasing the particle size, the saturated magnetization can increase with particles size. The decrease in the density of magnetization with the decrease in the average diameter of the nanocrystallites can be attributed to surface effects and core-shell morphology [47]. The decrease of the coercivity with increasing calcining temperature is attributed to the grain growth**.** The corecivity behavior indicates that Co atoms in the Fe-O matrix increase magnetic anisotropy of the material [48]. The as-prepared nanoparticles possess gradually decreased saturation magnetization in the order as calcined $CoFe_2O_4$> SC > TSC, indicating the strong magnetic property of the present nanoparticles. The decreased magnetization values for both supported SC and TSC are mainly due to the contribution of the volume of the non magnetic coating layer to the total sample volume. It is noted that the non magnetic coating layer can be considered as a magnetically dead layer over the surface of $CoFe_2O_4$ particles thus affecting the magnitude or uniformity of magnetization due to quenching of surface moments. Additionally, the values of $M_s$decreased with increasing the content of TiO_2 in the composite TiO_2/ $CoFe_2O_4$, because of the contribution of the volume of the non-magnetic coating layer to the total sample volume. Moreover, the remnant magnetism of the prepared particles fades to zero when the intensity of applied magnetic field weakens to zero. This reduce the aggregation of catalyst after it was separated by applied magnetic field from original reaction solution, so the photocatalyst can be easily re-dispersed in a solution for reuse after the external

magnetic field is eliminated. It indicates that the photocatalyst can be separated easily from wastewater by an external magnetic field because of their low M_r values [49].The saturation magnetization and remenant magnetization increased with increasing heat-treatment temperatures for sample TSC-300 as shown in Table 3. This happened because of the incomplete crystallization and small particle size after treating at low temperatures.The increase of the coercivity with increasing calcining temperature is attributed to decrease grain growth**.**

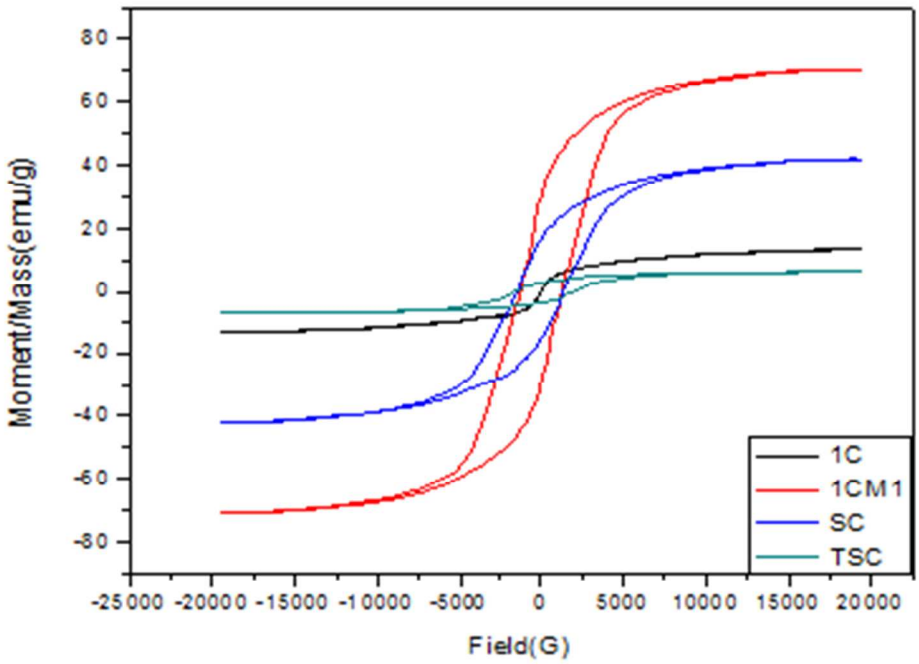

Figure 8: Magnetization vs applied magnetic field for 1C,1CM1,SC, and TSC at room temperature.

Table 2: Magnetic properties of as prepared magnetic nanoparticles and its composites.

Sample	Corecivity , Hc, (*kOe*)	Remnant magnetization ,*Mr*, (emu/g)	Saturation Magnetization , *Ms*, (emu/g)
1C	0.02	0.3	13.6
1CM1	1.25	29.49	70.63
SC	1.5	16.97	42.1
TSC	1.68	3.1	6.53

TSC-300	1.7	3.3	7.0

3.5. Problems affecting photoactivity when TiO_2 contacts to iron oxides.

3.5.1. Photodissolution of iron oxides.

The low photoactivity of iron oxide/ titania systems has been observed by Meron et al [48] as well as the observed high levels of photodissolution of this sample suffered from upon illumination with near UV light. Electronic interactions occur at the point of contact of between these two semiconductors (heterojunction), leading to the transfer of charge carriers across this junction, when two or more semiconductors are in contact that it were the major contributing factor for the reduced photoactivity [7].

The first possible source is the photodissolution of Fe ions which had diffused into the TiO_2 coating during the heat treatment step. The second possible source is the photodissolution of interfacial Ti–Fe oxides compounds formed during the heat treatment step due to a reaction between titanium dioxide and iron oxide phases. Finally, the third possible source is the direct photodissolution of the iron oxide core itself. Fe ion diffusion into the TiO_2 matrix during the heat treatment of TiO_2 and iron oxide phases in contact, leading to an Fe-doped TiO_2 lattice [50].

3.5.2. Electron-hole recombination.

The narrower **band gap** of the iron oxides is thought to lead to an increase in the incidence of electron-hole recombination, lowering the photoactivity, while the continuous hopping between Fe^{2+} and Fe^{3+} in the magnetite lattice has been reported to enhance electron–hole recombination. The lower oxidising power and reducing power of the of the available electrons and holes once transferred to the iron oxide phase can also be translated into lower photoactivity [7].

3.5.3. Aggregation.

The magnetic photocatalyst particles showed serious aggregations in water: an average aggregate size of 650 nm is observed while P25 particles mainly maintain a good dispersion condition [51].

Papers reporting TiO_2 coating onto magnetite (Fe_3O_4), maghemite (γ-Fe_2O_3), or ferrite (MFe_2O_4 where M is a divalent cation) cores, rather large or aggregated particles. When used as magnetic photocatalysts. The activities of these materials are generally low. This was explained by an

unfavorable electronic interaction between the TiO_2 shell and the magnetic core, leading to an increase in electron-hole recombination.

3.6. Photocatalytic Studies.

The photodegradation of dichlorophenol-indophenol (DCPIP) in aqueous solution over different powder samples is plotted against UV or visible irradiation time. Experimental results showed that the corresponding data fit the Langmuir–Hinshelwood (L–H) kinetic model (equation 4):

$$1 / r = 1/ k_r + 1 / (k_r K C) \qquad (4)$$

where r is the decomposition rate of the reactant (mg L^{-1} $min.^{-1}$), C is the concentration of the reactant (mg l^{-1}), t is reaction time (min.), K is represents the equilibrium constant for adsorption of the dye on TiO_2 particles (Langmuir constant) and k_r represents the specific reaction rate constant for the oxidation of the reactant (mg l^{-1} $min.^{-1}$) [52]. However, adsorption/desorption equilibrium is to be established under irradiation and in catalysis achievements, which is a major issue requirement for the validity of the L–H model.

When the chemical concentration C is millimolar solution, the integrated form of equation (5) to be an apparent first order equation:

$$\ln (C_o/C) = k_r K\, t = k_{app}\, t \qquad (5)$$

where k_{app} represents apparent first order rate constant of the photocatalytic degradation. A plot of ln (C_o/C) versus time represents a straight line, the slope of which upon linear regression equals the apparent first order rate constant (k_{app}). Generally, first order kinetics is appropriate for several studies were reasonably well fitted by this kinetic model

The half life time ($t_{½}$) of the first order reaction is the time required for the reactants to be degraded to the half of their initial concentration. The relationship between $t_{½}$ and k_{app} is given by equation 6.

$$t_{½} = 0.693/ k_{app} \qquad (6)$$

3.6.1. Photocatalytic activity for DCPIP degradation by UV and Visible illumination.

Figure 9,10 and Table 3 show the photocatalytic degradation curves of DCPIP dyeover the prepared pure anatasemesoporus TiO_2, $CoFe_2O_4$, TSC, TSC-300 and Degussa P-25 under UV and visible irradiation, respectively with a constant dye concentration of about $1x10^{-4}$ M, catalyst loading about 1g /L TiO_2at natural pH at 6.7.It was found that Degussa P-25 and TSC core–shell-shell structures show a low photocatalytic efficiency under identical UV-light exposure compared with 4C (The highest efficiency) at curve f . TiO_2 with high crystallinity is characterized by longer charge carrier lifetime thus associated with more efficient electron–hole utilization and decrease in the content of amorphous TiO_2; thus, increasing the photocatalytic activity of TiO_2. High degree and quality of crystallization means the presence of fewer TiO_2 bulk defects, where photoexcited electron and holes can recombine. Meanwhile the porosity and surface hydroxylation affect the transport and higher capacity of oxygen adsorption on the catalyst active site [53]. However, the anatase nanocrystal-coated samples (the calcined $CoFe_2O_4/SiO_2/TiO_2$ core – shell structures) exhibit high photocatalytic efficiency, which is comparable to that of well-known commercial photocatalyst Degussa P25 under visible light exposure. The apparent first-order photodegradation rate constant of TSC is 0.0325 and $0.0514min^{-1}$ under UV and visible irradiation, respectively**.** The photodegradation rates of these photocatalysts under UV illumination obey the following order:4C > P25 > TSC>TSC-300 >$CoFe_2O_4$ >UV alone and under visible illumination follows the order: 4C > TSC>P25>TSC-300>$CoFe_2O_4$> visible alone. In Figure 9 and 10, curve (a) shows that UV and Visible alone have no photocatalytic activity. Curve (b) shows that $CoFe_2O_4$ has a little photocatalytic activity under UV irradiation.The bad influence of the $CoFe_2O_4$ cores and the function of the silica partition under visible light irradiation are similar to those under UV irradiation. Strong light absorption of the $CoFe_2O_4$ cores under either UV or visible irradiation is one of the important reasons for the lower photocatalytic activity of the loaded catalyst. Because of the strong absorption of the $CoFe_2O_4$ cores, the self-photosensitization of the dye was markedly weakened, and the discoloration of the dye under visible irradiation by $CoFe_2O_4$ (curve (b)) was much slower than that in the blank reaction (curve (a)). The photocatalytic activity of TSC (curve c) is lower than P-25 (curve e) under UV illumination. This may be due to an effective recombination center of electrons and holes occurred by $CoFe_2O_4$ andsilica didn't form a complete membrane around the surface of cobalt ferrite nanoparticles. TSC-300 (curve d) has slower

photodegradation rate constants than titania under UV and visible illumination. The slower photocatalytic activity of the magnetic composite particles can be ascribed to the absorption of a portion of the incoming UV light by cobalt ferrite magnetic cores. This optical screening effect decreases the amount of the available UV light energy, which will serve to produce active holes and electrons in titania, eventually slowing the overall photocatalytic activity. This clearly shows the effect of the improved crystallinity after the heat-treatment. The apparent first-order kinetic equation $\ln (C_o/C) = k_{app}\, t$ was used to fit experimental data. The kinetic curve in Figure 11 and 12 are first order. Therefore, the apparent rate constant was chosen as the basic kinetic parameter for the different photocatalysts since it enables one to determine a photocatalytic activity independent of the previous adsorption period in the dark and the concentration of DCPIP dyeremaining in the solution. The apparent rate constant for prepared titania (4C), Degussa P-25, TSC, TSC-300, $CoFe_2O_4$ and blank under UV and Visible radiation are shown in Table 36, respectively.

The poor efficiently of photocatalyst (TSC, TSC-300) can be attributed to trapping of photogenerated carriers at the trapping sites produced in the titania lattice due to metal ion doping during annealing of photocatalyst or to the direct injection of charge carriers from photocatalytic shell into the core that shunts the charge carriers away from solid-solution interface and promotes recombination with a net reduction in photoreactivity.

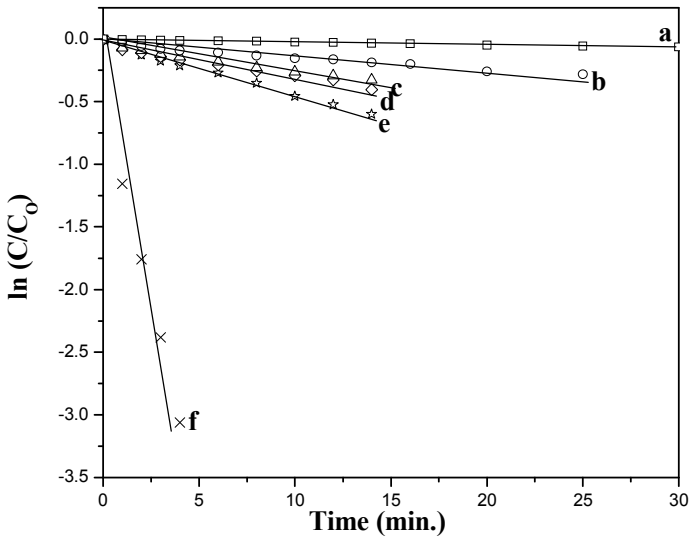

Figure 9: Kinetics of DCPIP dye disappearance in the presence of a) UV alone , b) Calcined $CoFe_2O_4$, c) TSC , d) TSC -300 , e) Degussa P-25 , and ., f) 4C under UV illumination .

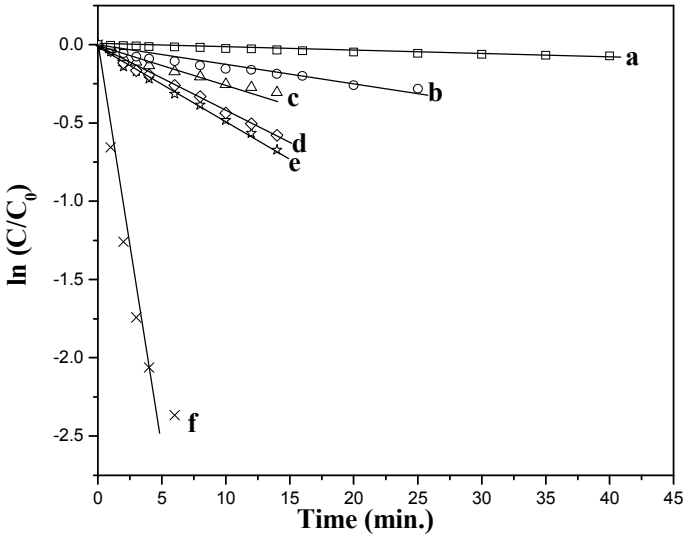

Figure 10 : Kinetics of DCPIP dye disappearance in the presence of a) Visible alone , b) Calcined $CoFe_2O_4$, c) TSC-300 , d) Degussa-P25 , e) TSC , and ., f) 4C under Visible illumination .

721 **Table 3: Kinetic parameters, effect of UV and Visible light of photodegrdation of DCPIP**
722 **dye using a bench scale batch photoreactor.**

Catalyst	Catalyst conc. (g/L)	DCPIP conc. (10^{-4}M)	pH	Type of Light	Apparent rate constant k_{app} (min^{-1})	$t_{½}$ (min.)
4C	1	1	6.7	UV	0.862	0.804
				Visible	0.544	1.274
TSC	1	1	6.7	UV	0.0326	21.26
				Visible	0.05144	13.47
TSC-300	1	1	6.7	UV	0.025	27.78
				Visible	0.030	23.1
Degussa P-25	1	1	6.7	UV	0.0459	15.10
				Visible	0.0436	15.89
$CoFe_2O_4$	1	1	6.7	UV	0.0133	52.01
				Visible	0.0132	52.44
Without TiO_2	---	1	6.7	UV	3.86×10^{-3}	179.53
				Visible	2.4×10^{-3}	285.26

723

3.6.2. Differences of photocatlytic degradation between UV and Visible irradiation.

Utilize the solar light (xenon light is similar to the solar light), Sunlight is abundantly available nature energy source, its energy can be conveniently exploited for the irradiation of semi-conducting materials. What is more, UV source is not only hazardous but also expensive because of the large input of electric power to generate UV irradiation. So, it is worthy of further research about how to make sunlight to be the ultimate source [54]. The photodegradation rates of these photocatalysts under UV illumination obey the following order: 4C > P25 > TSC>TSC-300 >$CoFe_2O_4$ >UV alone and under visible illumination follows the order: 4C > TSC>P25>TSC-300>$CoFe_2O_4$> visible alone.

This can be attributed to the difference in the photocatalytic mechanisms of DCPIP under UV and visible irradiation. **Under visible irradiation**, the DCPIP molecule can be excited to appropriated excited states, then the excited DCPIP undergoes reactions by two concurrent routes: (1) A route involving singlet oxygen, which was generated by energy transfer from the excited DCPIP molecule to ground state oxygen, then the DCPIP molecules are oxidized by the singlet oxygen; it can be seen from the data of degraded DCPIP in the blank reaction (in the absence of any solids). (2) Electron transfer from an excited state of DCPIP to the conduction band of titania particles, and the injected electrons of the semiconductor can react with the adsorbed oxygen to form oxidizing species which can bring about the photo oxidation of DCPIP In the presence of TSC and P-25, it may be both undergo the photosensitized degradation of DCPIP molecule. In addition, it can observe that the DCPIP may be show the activity of iron dopedtitania which had been proved has visible-light-induced photocatalytic activity. Therefore, the photocatalytic activity of P25 was much lower than DCPIP under visible irradiation. **Under UV irradiation**, although the photo-sensitization process of the DCPIP still exists to some extent, it is titania but not the DCPIP molecule that mainly absorb the photon with energy larger than the band gap of titania to generate electrons and holes in the conduction and valence bands, respectively. Then the photogenerated holes can react with adsorbed hydroxy or H_2O to form hydroxyl radicals which can oxidize the DCPIP molecule. While the photogenerated electron can react with the adsorbed oxygen yield superoxide radical anion which can also oxidize the DCPIP molecule [55].

4. Conclusion.

Magnetic nano composites ($CoFe_2O_4$ / SiO_2 / TiO_2) was successfully prepared by coating of $CoFe_2O_4$ as magnetic core with an insulating silicon dioxide (SiO_2) layer and photocatalytic properties of the outer titanium dioxide shell with crystal size 5.8 nm to solve problem of separation of photocatalyst and Visible range . Also, highly active TiO_2 nanoparticles with anatase phase and 6 nm average crystallite size has been successfully synthesized via sol-gel/hydrothermal route with acidic condition with Teflon lined stainless steel autoclave. The as-synthesized nanocomposites and TiO_2 were examined for the degradation of DCPIP dye in an aqueous solution. Based on the results achieved, it is concluded that the photodegradation rates of these photocatalysts under UV illumination obey the following order: 4C > P25 >TSC >TSC-300>$CoFe_2O_4$> UV alone and under visible illumination obey the following order: 4C > TSC>P25>TSC-300 >$CoFe_2O_4$> visible alone. The maximum level reached for the degradation of the dye molecule was 95.32 % for 3 min under TiO_2 loading 1g/l , 1×10^{-4} M of dye, natural pH under UV illumination and 87.27 % for 4 min the same condition under visible illumination. The present magnetic photocatalyst is expected to demonstrate a broad range of utility for other catalytic reactions which needs further investigation.

Acknowledgment

This work has been done under the project funded bythe Science and Technology Development Fund (STDF), Ministry of Scientific Research, Project ID: 1414, “Quantum Dots Nanomaterials Dye Sensitized Solar Cells”.

5. References.

[1] X. Bai, X. Zhang ,Z. Hua, W. Ma, Z. Dai, X. Huang, H. Gu , *J. Alloy Compd.,* 2014, **599**,10;

[2] J. Q. Xiang, K. Lv, J. G. Yu, *Appl. Catal. B: Environ.,* 2010, **96**, 557;

[3] T.Y. Leung, C.Y. Chan, C. Hu, J. C. Yu, P.K. Wong, *Water Res.,* 2008, **42**, 4827;

[4] K. Pomoni, A. Vomvas, C. Trapalis, *Thin Solid Films,* 2005, **479**, 160;

[5] A. AbdAziz, K. S.Yong, S. Ibrahim, S. Pichiah, *J. Hazard. Mater.,* 2012,**199**,143;

[6] R.L. Pozzo, M. Baltanas, A. Cassano, *Catal. Today*, 1997, **39**, 219;

[7] D. Beydoun, R. Amal, *J. Mol. Catal. A: Chem.,* 2002, **180,193**;

[8] A. Yanhui , X. Jingjing , Z. Songhe , F. Degang, *J. Phys. Chem. Solids,* 2009, **70**, 1042;

[9] L. Seung , D. Jack, M. David, Y.W. Chang , M.S. Wolfgang, *Mater. Chem. Phys.,* 2006, **96**, 483 ;

[10] O. Mohanta, Y. N. Singhbabu, S. K. Giri, D. Dadhich, N.N. Das, R. K. Sahu, *J. Alloy Compd.,* 2013, **564** , 78;

[11] P. Maa, W. Jianga, F. Wang , F. Li, P. Shen, M. Chen, Y. Wang, J. Liu, P. Li , *J. Alloy Compd.,* 2013, **578**, 501;

[12] M. Shokouhimehr, Y. Piao, J. Kim, Y. Jang, T. Hyeon, *Angew. Chem. Int. Ed.,* 2007, **46** ,7039;

[13] S. Pauline, A. P. Amaliya, *Arch. Appl. Sci. Res.*, 2011, **3**, 213;

[14] S.R. Ahmed, Dissertation for Doctor of Philosophy to the Faculty of the Graduate School University of Maryland, USA, 2002,

[15] V. Spelak, D. Schultze, F. Krumeich, U. Steinike, K.D. Becker, *Solid State Ionics*,2001, **141–142** , 677;

[16] J. Chen, Y. Wanga, Y. Deng, *J. Alloy Compd.*, 2013, **552**,65;

[17] A. M. Ibrahim, M.M. Abd El-Latif, M.M. Mahmoud, *J. Alloy Compd.*, 2010, **506**,201;

[18] H. A. Hamad, M. M. Abd El-latif, A. B. Kashyout, W. A. Sadik, and M. Y. Feteha , *Russ J Gen Chem.*,2014,84,2031;

[19] H. Zhang, R. Qi, D. G. Evans, X. Duan, *J. Solid. State Chem.*, 2004, **177**,772;

[20] M. A. Lakraimi, A. Legrouri, A. D. Barroug, J. P. Roc, J. P. Besse , *J. Mater. Chem.*, 2000, **10**, 1007 ;

[21] H. Jing, W. Min, B. Li, Y. Kang, G.E. David , D. Xue, *Struct. Bond*, 2006, **119**, 89;

[22] B. Donia, A. Rose, L. Gary, M. Stephen, *J. Mol. Catal. A: Chem*., 2002,**180**, 193;

[23]P. Gherardi , E. Matijevic, *J. Colloid. Interf. Sci.*, 1986, **109**, 57;

[24] S. Watson, D. Beydoun, J. Scott, R. Amal, *J. Nanopart. Res,* 2004, **6**, 193;

[25] H. Zhang, J.F. Banfield, *J. Phys. Chem. B*, 2000, **104**, 3481;

[26] R. P. Bacsa, J. Kiwi, *J. Appl. Catal. B: Environ.*, 1998, **16** ,19;

[27] J. Yuan, Y.K. LÜ, Y. Li, J. Li, *Chem. Res. Chinese U.*, 2009, **26**, 278;

[28]E.J.A.Pope, J. D. Mackenzie, *J. Non-Cryst. Solids*, 1986, **87**,185;

[29] A.V. Korzhak , N. I. Ermokhina , A. L. Story, A.K. Bukhtiyarov, A.E. Raevskaya , V.I. Litvin, S.Y. Kuchmiy, V.G. Ilyin, P.A. Manorik, J. Photochem. Photobiol. A, 2008, **198**, 126;

[30] S.M. Chang, R.A. Doong, *J. Phys. Chem. B*, 2006, **110**, 20808;

[31] Y. Wu, J. Zhang, L. Xiao, F. *Chen, Appl. Surf. Sci.*, 2010, **256**, 4260;

[32] L. Seung, D. Jack , M. David, Y.W. Chang, M.S. Wolfgang, *Mater. Chem. Phys.*, 2006, **96**, 483;

[33] H.G. Yang, H. C. J. Zeng, *Phys. Chem. B*, 2004,**108**, 3492.

[34] S. Watson, D. Beydoun, R. Amal, *J. Photoch. Photobio. A*, 2004, **148** ,303;

[35] Z. Y. Liu, X. Quan, H. P. Fu, X.Y. Li , K. Yang , *Appl. Catal. B*, 2004, 52, 33;

[36] F. Cot, A. Larbot, G. Nabias, L. Cot, *J. Eur. Ceram. Soc.,* 1998, **18**, 2175;

[37] M. R. Hoffmann, S. T. Martin, W. Choi, D.W. Bahnemann, *Chem. Rev.*, 1995, **95**, 69 ;

[38] B. D. Cullity, *Introduction to Magnetic Materials, Addison-Wesley Publishing*, 1972;

[39] X. Huang, Z. Chen, *J. Cryst. Growth*, 2004, **271**, 287;

[40] L.J. Zhao, S.S. Yan, B. Z. Tian, J.L. Zhang, M. Anpo, *Mater. Lett.*, 2005, **60,** 395;

[41] S. Iimura, H. Teduka, A. Nakagawa ,S. Yoshihara, T. Shirakashi, *Electrochemistry,* 2001, **69**, 324;

[42] B. A. Morrow, J. L. G. Fierro , *Spectroscopic Characterization of Heterogeneous Catalysis Elsevier Science Publishers, Amsterdam*, A161, 1990;

[43] Y. D. Hou, X. C. Wang, L. Wu, X. F. Chen, Z. X. Ding, X.X. Wang, X.Z. Fu, *Chemosphere,* 2008, **72** , 414 ;

[44] S. Music, M. Gotic, M. Ivand, S. Popovic, A. Turkovic, R. Trojko, A. Sekulic, *Mater. Sci. Eng. B*, 1997, **47**, 33 ;

[45] H. Zhang, R. Hou, Z. Lu, X. Duan, *Mater. Res. Bull.*, 2009, 44, 2000;

[46] K. Chhor, J. F. Bocquet, C. Pommier , *Mater. Chem. Phys.*, 1992, **32**, 249;

[47] R.H. Kodama, A. E. Berkowitz, E. J. McNiff, S. Foner, *Phys. Rev. Lett.*, 1996, **77**, 394;

[48] T. Meron, Y. Rosenberg, Y. Lereah, G. Markovich, *J. Magn. Magn.Mater.,* 2005, **292** , 11;

[49] Y. Jin, L. Yong-kang, L.Yu, L. Jun-ping, *Chem. Res. Chinese U*, 2010, **26**, 278 ;

[50] J. Huang, T. Shinohara, S. Tsujikawa, *Zairyo-to-Kankyo*, 1997, **46**, 651;

[51] W. Qiu, Y. Zheng, K.A. Haralampides, *Chem. Eng. J.,* 2007, **125**, 165;

[52] S. M. Chang, R.A. Doong, *J. Phys. Chem. B,* 2006, **110**, 20808 ;

[53] Z. W. Liu, X. Quan, H.P. Fu, X.Y. Li, K. Yang, *Applied Catalysis B* ,2004, **52**,33;

[54] X. Lou, J. Han, W. Chu, X. Wang, Q. Cheng, *Mater. Sci. Eng. B,* 2007, **137**, 268;

[55] X. Huang, Z. Chen, *J. Cryst. Growth*, 2004, **271**, 287;

Graphical Abstract

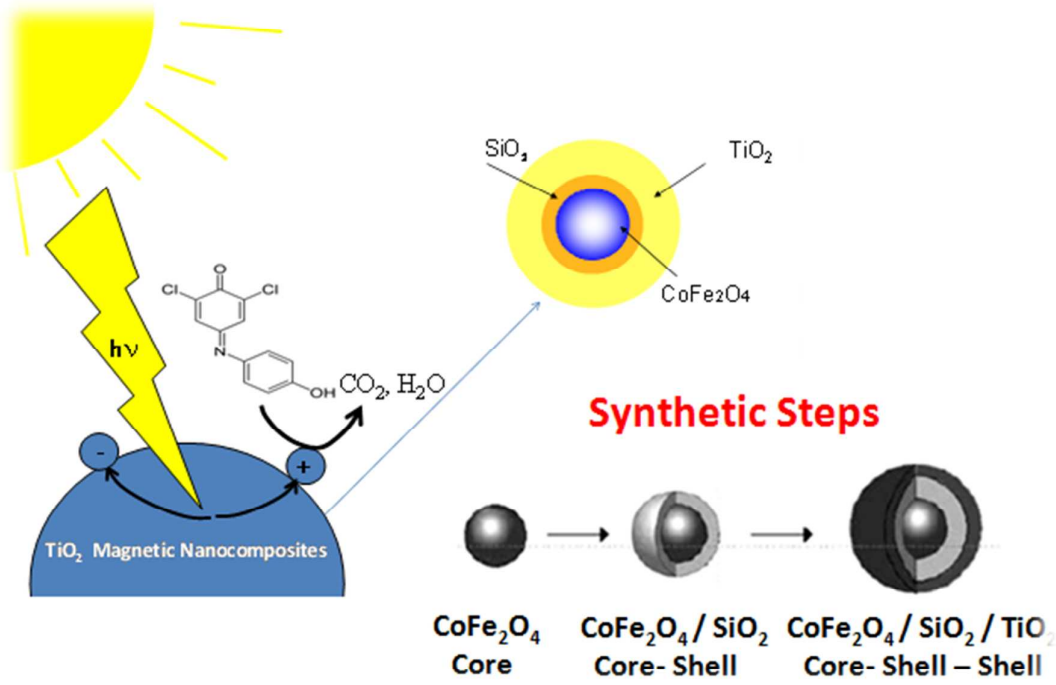

$CoFe_2O_4/SiO_2/TiO_2$ core-shell-shell magnetic nanocomposites have been prepared by coating of cobalt ferrite nanoparticles with the double layers of SiO_2/TiO_2.